THE ENERGETICS OF COOLANT-BUBBLE-COVERGAS INTERACTIONS ASSOCIATED WITH LMR OUT-OF-REACTOR SOURCE TERM EXPERIMENTS

John C. Petrykowski*, Hamza Mohamed
University of Dayton
300 College Park Drive
Dayton, Ohio, USA
jpetrykowski1@udayton.edu

ABSTRACT

In certain extremely low probability, severe accident scenarios which have been postulated for liquid metal cooled fast reactors, large bubble cavities containing fuel vapor and fission products transit a layer of coolant and release this material to the cover gas thereby presenting a contribution to an accident-specific source term. So that a more mechanistic assessment of these types of events can be developed, analyses have recently been performed to account for the heat and work transfer observed in out-of-reactor source term experiments conducted during the 1980's for oxide fueled reactors in the Fuel Aerosol Simulant Test (FAST) facility at Oak Ridge National Laboratory. In ten experiments, UO_2 specimens were vaporized in pools of sodium, and for an additional number of benchmarking tests, in pools of water, for purposes of experimentally assessing the bubble transport characteristics of both types of pools. The current analyses present several firsts for these experiments: (a) a comparison of the bubble-to-coolant transfer rates; heat versus work, (b) a bubble-to-coolant heat transfer model accounting for how condensation and radiation heat transfer are affected by coolant selection; sodium versus water, and (c) an assessment of how both types of heat transfer influence the movement of aerosol-laden bubbles through the coolant pool. These analyses significantly extend previous evaluations of FAST experimental results by providing a more comprehensive model for determining how bubble-coolant interactions affect aerosol transport and, in this way, contribute to data base development associated with mechanistic assessments of the source term.

KEYWORDS
Safety, accidents, thermalhydraulics, extreme events.

1. INTRODUCTION

It is generally recognized that safety considerations for liquid-metal cooled reactors differ sufficiently from light water cooled reactors so that the safety case put forward during licensing would necessarily draw on specific pre-licensing activities that pertain to the liquid-metal cooled systems. Recent studies [1-4] regarding hypothetical, severe accident events in sodium-cooled as well as lead-cooled configurations have considered the impact on accident progression of the formation and presence of vapor bubble cavities within the coolant, where the cavities may contain various mixtures of fission products, combined in some cases with fuel, coolant and structural materials. Portions of each component may be in aerosol form. Because of the type of fuel relocation that takes place, the events are referred to as core disruptive accidents (CDA). Although the probability of these accidents is extremely low the potential radiological consequences could be significant. For this reason there is continued awareness, particularly at the regulatory level [5], regarding the importance of examining certain phenomenological aspects of this accident type particularly when those aspects could impact an assessment of the radiological hazard that the accident exposes, the quantification of which is referred to as the source term.

Source term considerations differ widely based on the severity of core disruption so it is important to distinguish between two distinct category types, (1) a core melt type of disruption in which the initiation

phase may be localized to a single fuel pin and may potentially occur in both metal fueled as well as oxide fueled reactors and (2) a more energetic type of core disruptive behavior thought to be more probable in oxide fueled reactors. For this second type of disruptive accident, significant fractions of fuel inventory could undergo a vaporization process that would lead to formation of large fuel-vapor bubbles. Bubbles in both types of disruptive accidents could undergo transport to the covergas through the available coolant. Examples of safety studies which focus on these accidents include modelling activities [1] and experimental activities [6] respectively. Details of event progression can be found in these studies. The focus of this paper is to provide an assessment of data [7,8] obtained from out-of-reactor source term experiments designed at Oak Ridge National Laboratory in the 1980's, conducted in the Fuel Aerosol Simulant Test facility and pertinent to the energetic-type CDA.

The main objective of the present study is to place the assessment of the data on a more mechanistic footing. The experiments were designed to examine, primarily on a phenomenological basis, the transport to a covergas space of a bubble containing simulant oxide-fuel vapor and fission product mixtures. Bubble formation occurred during capacitor discharge vaporization (CDV) of simulant material positioned in sodium pools. In what follows it will be shown that the transport characteristics of the bubble were consistent with the energy transfer that occurred between the pool, the bubble and the covergas. Additionally, a condensation heat transfer model is presented which permits an identification of radiation as the dominant heat transfer mode. Finally the development and implementation of a work transfer model permitted a rank ordering of the energy transfer processes so that some of the temporal features of the bubble could be attributed, in part, to heat transfer effects which were present during the experiments.

The methodology needed to assess these three items requires supporting information: experimental facility and test plan, principle measurements associated with the observed bubble dynamic behavior, modelling activities associated with the energetics of the experiment and an assessment of how vapor and aerosol transport may have most likely progressed in light of the available data and the modelling predictions. These items are discussed in the following sections.

2. EXPERIMENTAL FACILITY AND TEST PLAN

The following components comprised the FAST facility: (1) the FAST vessel and associated hardware and measurement equipment, (2) the vaporizer unit in which the UO2 sample was initially contained, and (3) the CDV power supply system used to energize the sample. The FAST vessel and measurement equipment are shown schematically in Fig. 1. The vessel was ~1.83 m high and ~.61 m in outer diameter and had an internal volume of ~0.46 m^3. The vessel was fabricated from 0.022-m-thick 304 H stainless steel. The design temperature limit of the vessel was 880 K; the design pressure limit was 3.08 MPa. Heaters were used to regulate temperature from 363 K (for several preliminary water tests) to 811 K for tests in sodium.

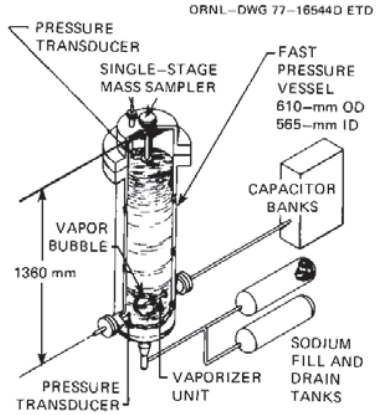

Figure 1. The FAST test facility

The vaporizer unit, shown schematically in Fig. 2, includes electrodes, a UO_2 sample, and sample holders. A sample consisted of 13 UO_2 pellets (4.85 mm-dia.) stacked end-to-end having a total mass of ~17.3 g and an overall length of ~90 mm. The pellet stack was surrounded by ~32 g of UO_2 microspheres [300 to 500 μm (diameter)] which were used to thermally insulate the pellets. Electrical contact with the power supply was maintained by electrodes at the ends of the pellet stack. Axial and circumferential grooves were scribed on the external surface of the vaporizer unit to provide fracture sites for efficient rupture during the capacitor discharge. In addition, the vaporizer unit was charged with xenon to simulate fission products.

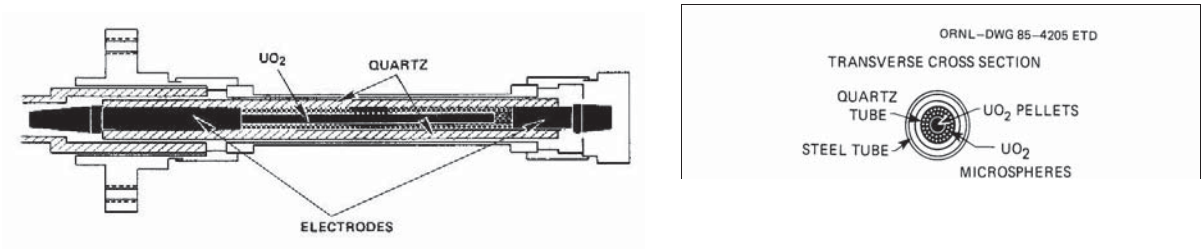

(a) (b)

Figure 2. The FAST vaporizer unit in cross-section: (a) longitudinal, (b) transverse.

During heating, power levels trended from ~1.6 kW during preheat, consistent with levels needed to bring about localized UO_2 melting, to peaks of ~10 MW during discharge which was sufficient to vaporize UO_2 and create a highly energetic disassembly.

As the sample disassembled, a dynamic mixture was formed containing UO_2 phases, xenon, vaporizer material and coolant. Pressures resulting from heat, mass, and momentum transfer between the mixture and the surrounding media were measured using transducers, one positioned axially 0.23 m from the vaporizer assembly, the other positioned radially, well above the vaporizer assembly, in the covergas. In all but one sodium experiment (FAST-111), the sodium pool covered the vaporizer and the resulting submerged mixture formed a multi-phase, multi-component bubble. The axially and radially mounted transducers measured the pool and covergas pressure, respectively. Covergas pressure measurements were also used to estimate both the size of the bubble as a function of covergas compression as well as the boundary-work* done on the covergas as it underwent compression as a result of bubble expansion. This work transfer was combined with heat transfer estimates computed from the analytical models so that the input energy (electric) could be compared to the output energy (work transfer/heat transfer) to arrive at an assessment of the overall energy budget.

The experiments conducted in the FAST facility used a variety of cover gas pressures and sodium pool and water pool levels, and in the water tests, a variety of pool temperatures as well, to determine what effect these parameters had on aerosol release to the cover gas. Although the pool level was one of the most critical experimental parameters affecting release as adjustments account for the physical extremes of low release, corresponding to high pool levels, to total release, corresponding to subvaporizer levels, subcooling of the pool was also recognized as an important contributor to suppressing bubble transport. For this reason, pool heating was used in several of the water tests to reduce subcooling to 15 K, a reduction of 70 K from normal operating conditions. Pool level settings spanned a wide range of values (-300 mm to +1060 mm; see Fig. 4(a)); the -300 mm pool level experiment (FAST-111) was designed to gauge the aerosol yield potential of CDV. Variations in argon pressure were used to determine the effect of cover gas compressibility on bubble size, pool dynamics and aerosol release. Covergas pressure varied over an order of magnitude during the series of experiments. Xenon pressure levels were varied to account for the effect of non-condensables on bubble transport. Values of experimental parameters, bubble size estimates and aerosol release levels are listed in Table I for selected experiments.

*Boundary work is mechanical work done, under the action of pressure, to move a boundary.

Table I. Parameters from Selected Experiments

Exp#/Fluid	Fluid Temp (K)	Covergas Vol. (m^3)	Covergas Press. (kPa)	Pool Vol. (m^3)	Pool Level (m)	Aerosol Mass (g)	Xe Press. (kPa)	Bubble R-max (m)	CDV Energy (kJ)
56/ H2O	359	0.090	122	0.37	1.12	0.014	515	0.13	30.4
64/ H2O	361	0.090	120	0.37	1.12	0.0063	515	0.14	35.2
66/ H2O	298	0.090	122	0.37	1.12	0*	515	0.09	29.2
68/ H2O	298	0.090	25	0.37	1.12	0*	515	0.20	33
104/Na	811	0.090	120	0.37	1.06	0.0003	133	0.10	37.4
105/Na	811	0.095	120	0.37	1.04	0.001	341	0.08	32.2
106/Na	811	0.30	120	0.16	0.24	0.0001	341	0.11	37.6
111/Na	811	0.45	122	0.014	-.300	1.1	341	†	22.8
112/Na	811	0.30	300	0.16	0.25	0.0009	338	0.06	26.5
113/Na	811	0.35	119	0.11	0.03	0.07	338	0.13	37

*In the water experiments, no aerosol mass was detected unless subcooling ≤ 15K.
†Vaporizer located in cover gas; no submerged bubble formed.

3. EXPERIMENTAL OUTCOMES

In this section, data is presented to corroborate the aerosol release fractions listed in column 7 of Table I. The data includes pressure traces from the coolant and covergas regions, semi-empirical estimates of bubble size and semi-empirical estimates of the work transfer delivered by the bubble to the covergas. This information will be used in conjunction with models of heat transfer, described in Section 4., to assay the energy budget associated with bubble transport through the coolant and to corroborate the observed levels of aerosol release from the bubble to the covergas. With regards to aerosol release, it should be noted that, with the exception of FAST 111 in which the vaporizer was positioned within the covergas, release of aerosol was very limited except in the case of two underwater tests (#'s 56,64) where the pool subcooling was significantly suppressed, in some cases, to as little as 10K. The primary purpose in the assessment that follows is to explain the relatively low release fractions that were evident, particularly in the sodium tests, with the noted exception of FAST 111.

3.1. Pressure-based Bubble Size Estimates

Pressure data, (see Fig. 3) were used in conjunction with the appropriate constitutive equation for the cover gas to estimate the maximum size of the submerged bubble. Estimates are reported in column 9 of Table I. An assessment of these values may illustrate to the reader why the series of experiments resists a single characterization based on bubble size attributes alone for although the reported bubble size characteristic at its smallest (FAST-112) is 25% of vessel radius, suggesting a large bubble size, volume sizing of a bubble as a percent of the total coolant volume yields values from 0.5% (FAST-112) to 10% (FAST-68) which, at the low end of this range, would suggest a "smaller" bubble size.

Regardless of the attributions that are used to qualitatively characterize bubble size, a common approach was adopted for computing an estimated maximum bubble size. One begins by assuming, based on negligible coolant compressibility, that covergas volumetric compression was matched by an equivalent volumetric expansion of the bubble. Further, assuming an isentropic compression of the covergas, it can be shown (see App. A) that the following formula can be used to represent the size of a hypothetical spherical bubble:

$$R = \sqrt[3]{\frac{3}{4\pi}\left(V_{B_0} + V_{cg_0}\left(1-(P_0/P)_{cg}^{1/\gamma}\right)\right)} \quad (1)$$

The initial bubble volume, V_{B_0} ,was assumed to be equivalent to the combined volume attributed to both intra-assembly gaps in the vaporizer between adjacent microspheres, and intra-assembly gaps in the vaporizer between the quartz and steel tubes. These gaps are depicted in Fig. 2 (b). The volume attributed to these gaps, assumed to be initially occupied by xenon, was taken as 15,000 mm^3. By extracting peak levels from the recorded covergas traces, eqn (1) was used to compute estimated maximum bubble size.

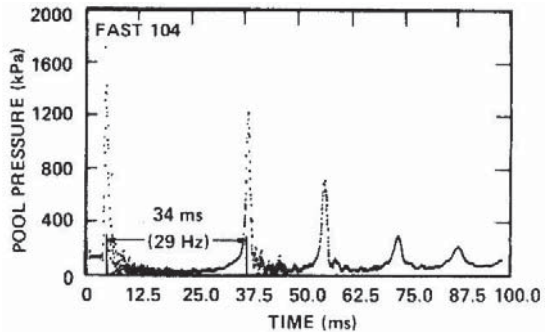

Figure 3 (a) Coolant pressure

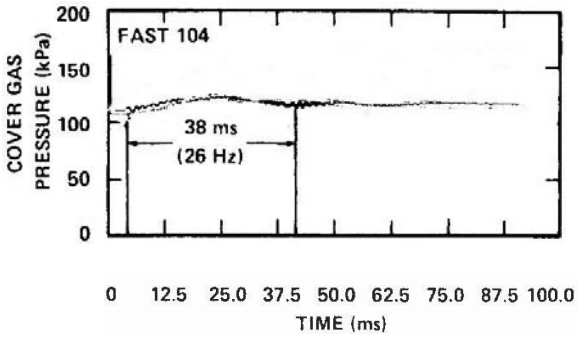

Figure 3 (b) Covergas pressure

With these calculations performed for every undersodium experiment, the metric $\eta = H/R_{max}$, adopted from bubble-pool studies of purely mechanical bubble pulsations [9], was then implemented for purposes of relating aerosol release measurements to bubble size measurements based on a characterization of bubble shape behavior as pulsatile about a stationary center. This highly-simplified view of bubble kinematics, i.e. that the bubble pulsated as a sphere and did not undergo translation, enabled the use of the following rubric for establishing a kinematic basis for aerosol presence in the covergas:

> $\eta = H/R_{max}<1$, aerosol release was more likely; venting of a "volatile bubble" to the covergas could be inferred based strictly on kinematic considerations,
>
> $\eta = H/R_{max}>1$, aerosol release was less likely; venting of a "volatile bubble" could not be inferred based strictly on kinematic considerations.

The trends suggested by this characterization are depicted in Fig. 4(b) and led to the conclusion that aerosol release was highly impeded in all but one undersodium experiment (FAST-113) because the volatile components of the bubble may have condensed out while the bubble was submerged within the pool.

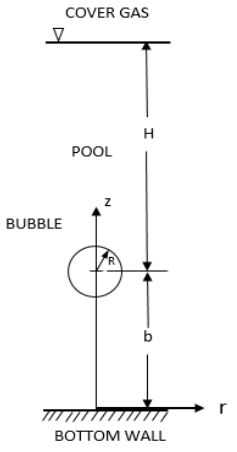

(a)

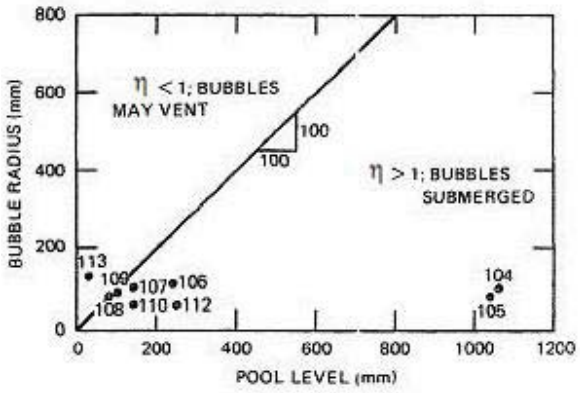

(b)

Figure 4. Bubble Position Relative to Pool Surface (a) Initially, (b) At R = R_{max} .

Because this characterization of bubble behavior corroborated the main aerosol trends , neither thermal hydraulic behavior of the coolant, bubble centroid movement, nor bubble surface deformation in response to coolant flow were considered in most of the remaining study.

3.2 Work Transfer

In the FAST experiments, work transfer, i.e., work done by the expanding bubble in compressing the covergas, could, if sufficiently large, cause components of the bubble to condense, perhaps shortening bubble lifetime or reducing the probability that a large bubble would reach the covergas. Although it is not reasonable to assume that work transfer alone could bring about complete elimination of high temperature vapor, if for no other reason than the bubble also contains non-condensable components, work transfer could reduce to some extent the amount of UO_2 vapor contained by the bubble as it reached the covergas. Since work transfer comprises one factor in the overall energy balance, the work transfer to the covergas could be computed using covergas pressure readings in conjunction with the boundary work formula,

$$W_{1\to 2(\theta)} = \int_1^{2(\theta)} P dV \tag{2}$$

where 1 represents the initial state of the covergas prior to firing the capacitor banks and 2(θ) represents some arbitrary state during the covergas compression process with θ representing the time that elapses in reaching this arbitrary state. To determine a lower-bound estimate as to how much work transfer took place up to the point of maximum covergas compression, eqn (2) was applied to the case of a maximum, isentropic compression of the covergas, for which the above formula becomes,

$$W = P_1 V_1 \left[\left(1 - \frac{4\pi R_{max}^3}{3V_1} \right)^{1-\gamma} - 1 \right] / (\gamma - 1) \tag{3}$$

where eqn (1) is used to compute R_{max} based on a covergas pressure value taken from the peak in the covergas pressure trace. To illustrate, in a comparative sense, the contribution of work transfer to the overall energy budget, data from underwater experiment 64, used in conjunction with equation (3) indicates that work transfer during the compression stage of the experiment reached 1545 J, or a 4.5 % share of the CDV energy input, suggesting that the preponderance of energy transfer was heat loss due to radiation or condensation. Whether similar claims could be made for the sodium experiments and whether those claims could be used to explain the low levels of aerosol release observed in those experiments is examined later in the context of a heat transfer assessment, the model of which is considered next.

4. HEAT TRANSFER MODELLING

A number of efforts have been previously directed at developing a means by which FAST experimental outcomes can be properly assessed, at various levels of detail. Studies accounting for heat transfer between the hot vapor bubble and the surrounding coolant include: (i) Ozisik and Kress [10] integral boundary layer analysis of a condensation heat transfer boundary layer in contact with the internal surface of the bubble, (ii) a more generalized, thermal-hydraulic formulation of Tobias [11-12] which added radiation to the results obtained in [10] to help assess how these sequential* modes affected the lifetime of a bubble buoying up through the sodium coolant and (iii) a hydrodynamic-thermal model of varying fidelity developed by Reynold's, et al., [13] which improved the geometric representation of the coolant-side heat transfer process through the use of a spherical boundary layer. Of these studies, no single case accounts for sequential heat transfer in the characteristic spherical cap shape that would be representative [14] of a buoyant bubble cooling to a volume of coolant thought to be representative of conditions prevailing in the FAST

*"Sequential" is used to denote that, condensation, as a thermodynamic equilibrium process, begins when, for a given bubble pressure, the bubble temperature reaches the saturation value, at which time the condensate film and the vapor are in thermal equilibrium, thus cutting out radiation heat transfer.

experiments. For example, [10-12] rely on non-representative bubble heat source forms in selecting a 1-dimensional, time dependent slab model to account for the coolant-side heat transfer while [13] does not include condensation heat transfer.

Regarding identification of a suitable interface shape for bubble-to-coolant heat transfer modelling, shape selection was guided by the aerosol-release bubble-motion correlations developed in this paper, the results of which were presented in Sect. 3.1, for which the aerosol release indicator η provided a means of correlating aerosol release. The correlation relied on an assumed, spherical bubble form. While the simplicity of the spherical shape was attractive from a modelling perspective there were additional rationales that could be advanced in arguing for a spherical form. For example, it is well known, from free-energy considerations, that an interface of spherical form offers shape stability over any other free-form candidate shape of equivalent surface area. Further, in the absence of direct physical interrogation of the surface of the bubble, and direct physical evidence was lacking owing to the opacity of sodium, there was no obvious basis for selecting a surface that would represent a departure from free-form. Further, bubble breakup into particular distributions or bubbleswarms could also not be easily inferred owing to the very energetic and uncontrolled insertion of the bubble into the coolant, a recognized [15] characteristic of CDV induced sample dis-assembly. Two additional assumptions, viewed as conservative from the basis of energetic assessments concerning the viability of a "volatile bubble", were imposed based on the notion that an overestimate of heat transfer will result in a conservative prediction of bubble time to extinction. The first assumption dealt with consideration of characteristic bubble size, the second dealt with considerations of time. Relative to the first consideration, a bubble of 0.05 m was selected as representative of the estimates of bubble size reported in Table I and relative to the second it was assumed that bubble size did not change throughout the process. Although this second assumption was clearly not consistent with known bubble behavior it provided a conservative estimate concerning bubble extinction, so it was adopted for the study presented here.

For these reasons, a model was developed which accounted for sequential heat transfer from a stationary, spherical bubble to a coolant space where the space exhibited a steady, spherical geometric form so that an account could be made of how radiation and surface condensation influenced the cooling of the bubble-types presumed present in the FAST experiments. Additionally of special interest is the elapsed time for heat transfer to the coolant, as this, relative to the rise time of the bubble, is a rough measure of the probability that a bubble condenses within the pool as opposed to breaking the surface and releasing bubble contents, including aerosols, to the covergas. Both of these metrics, sequential heat transfer and elapsed time, are objectives of the current heat transfer model. Because portions of the radiation heat transfer analysis have been documented [16], attention here is focused on surface condensation heat transfer as well as the development of metrics which provide a means for estimating, in a relative sense, the contributions to cooling of each heat transfer process.

In considering the extent to which condensation heat transfer effects the energy balance, a transient conduction heat transfer model was developed pertinent to the region $R \leq r < \infty$, which, as shown in Fig. 5, is the region associated with the bubble surface as well as the coolant. Neglecting such condensation related effects as fog formation or sputtering [17] one can develop a simplified model of the heat transfer problem. The thermal response of the coolant, if initially held at temperature T_i, and then instantaneously exposed at time $\theta = 0$ to surface heat flux q''_c at $r = R$, is governed by the system set

$$\alpha\nabla^2\varphi = \varphi_\theta, \qquad \varphi(r,0) = 0, \qquad -k\varphi_r\,|_R = h_c(\varphi_B - \varphi(R,\theta)), \qquad \varphi(\infty,\theta) = 0 \tag{4-7}$$

where $\nabla^2 = \frac{\partial^2}{\partial r^2} + 2r^{-1}\frac{\partial}{\partial r}$ is a variable coefficient form of the Laplacian operator, where $\varphi(r,\theta) = T(r,\theta) - T_i$ is the excess temperature and where h_c is the condensation heat transfer coefficient. Replacement by a constant coefficient operator can be achieved by the transformation $t = r\varphi(r,\theta)$, which converts (4-7) to an effective semi-infinite slab-type problem:

$$\alpha t_{rr} = t_\theta, \tag{8}$$

$$t(r,0)=0,\ \ -k(t/r)_r\ \big|_R = h_c((t_B-t)/r)\ \big|_R,\quad t(\infty,\theta)=0\ , \tag{9-11}$$

for the transformed temperature group, t. A self-similar formulation for the transformed temperature group, can be obtained via the similarity transformation $\beta = r(\alpha\theta)^{-1/2}/2$ which reduces (8-11) to:

$$\frac{d^2t}{d\beta^2}+2\beta\frac{dt}{d\beta}=0\ ,\quad -k(-t+\beta\frac{dt}{d\beta})\ \big|_{\beta_R}=R^2q''_c\,|_R\quad ,\ \ t(\infty)=0\ . \tag{12-14}$$

Two integrations of (12), with subsequent utilization of boundary constraints (13-14), yield an excess temperature of the form:

$$\varphi=(h_c\varphi_B R^2/(rk))\frac{erfc(\beta)}{(1+h_cR/K)erfc(\beta_R)+(2\beta_R/\sqrt{\pi})e^{-\beta_R{}^2}} \tag{15}$$

Because of numerical underflow conditions that can occur in evaluations of the complimentary error function for the large β conditions considered in this paper ($\beta_{Na} \approx 20$, $\beta_{H20} \approx 190$) the following large β asymptotic approximation [18] to (15),

$$\varphi=(2h_c\varphi_B\alpha\theta/(Rk))\cdot(R/r)^2\cdot e^{R\cdot(1-(r/R)^2)\cdot(R/(4\alpha\theta))}/(1+2\alpha\theta(1+h_cR/k)/R^2) \tag{16}$$

was developed for purposes of interpreting results. This formulation, plotted for coolant configurations pertinent to both sodium and water, is presented in Fig. 6 along with the solution [16] developed for the radiation heat transfer problem so that the relative importance of each heat transfer mode could be established.

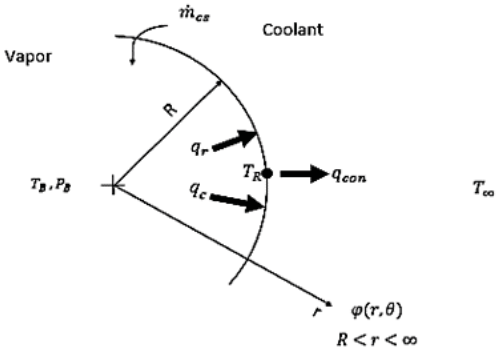

Figure 5. Modes of Heat Transfer

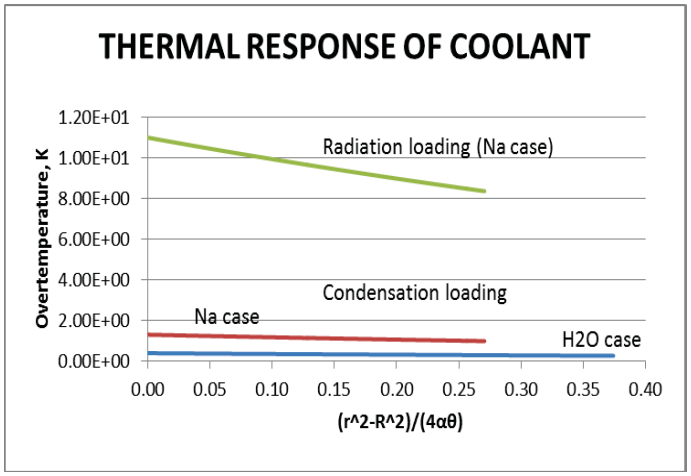

Figure 6. Predicted Temperature Trends

As a preliminary step in developing an energy-based rationale for assessing key experimental outcomes the soundness of the predicted thermal response must be evident. Several credible trends can be identified in the curves presented in Fig. 6:

(a) downward trending temperatures as the offset from the interface increases.
(b) in comparing temperature trends for the case of condensation heating, the responsiveness of sodium exceeds that of water.
(c) a temperature dimunition with offset from the interface that results in an e-fold reduction from interface temperature levels, where this e-folding length, δ, is given by

$$\delta = \frac{2\alpha\theta}{R} \tag{17}$$

The above trends (a-c) are consistent with what is commonly known regarding thermal systems of the type considered here and are supported by the following considerations:

- To the extent that heat transfer can be viewed as a proximity effect, the fall off of temperature with increasing distance from the source is a trend that would be expected.
- The thermal response, in a relative sense (sodium relative to water) favors sodium and is consistent with reported [19,20] thermophysical property data for each coolant. Specifically, sodium pools heat up faster due to a relatively small volumetric thermal inertia (i.e., $(\rho c_P)_{Na}$ = 0.98MJ/m^3-K, $(\rho c_P)_{H20}$ = 4.18MJ/m^3-K).
- Thermal energy is redistributed through the coolant by heat diffusion. Since a characteristic of many diffusion problems is an exponentially decaying effect, an e-folding characteristic could be inferred. Simple dimensional arguments point to an e-folding length of order αθ/R which is parametrically similar to the stated 2αθ/R e-folding length reported here.

An interpretation of the aerosol release data using the thermal response predictions is the focus of the next section.

5. ENERGY PATHWAYS AND ENERGY BALANCE ASSESSMENTS

The assessment of aerosol release in Sect. 3.1 is semi-empirical. The assessment is purely kinematic; bubble size estimates are used in conjunction with position of the vaporizer relative to the free surface to assess whether a growing, stationary bubble would break the free surface and vent aerosol material into the covergas. In what follows, the temporal effects of a rising, thermally-active bubble are compared with previous assessments of boundary work and heat transfer for purposes of determining whether sufficient time is available for a travelling bubble to break the coolant-covergas free surface or whether bubble lifetime is sufficiently short such that the bubble remains wholly submerged during the energy transfers so that little if any aerosol material could be expected to vent into the covergas.

Specifically, a comparison is made of two time scales: (1) a bubble rise time estimate, based on bubble size and bubble depth assuming a Taylor model [21] of buoyant motion and, (2) a bubble "extinction time" estimation based on the energy assessments for work and heat introduced in Sect. 3.2 and Sect. 4. If the extinction time in relation to the rise time is sufficiently short it would be anticipated that, with the possible exception of transport by the non-condensable component (i.e., xenon), little if any aerosol would be released to the covergas.

While estimates of the elapsed time for the boundary work range from 50 to 75 ms, as suggested by the covergas record (see Fig. 3 (b)), temporal estimates of heat transfer can be inferred from time integrations of the surface heat transfer, for each heat transfer mode, yielding, respectively,

$$Q_c = 4\pi\, h_c \varphi_B R^4 \left\{\left[(h_c R/k)/(1+\left(\frac{h_c R}{k}\right))\right] \ln\left(1+2\cdot\left(1+\left(\frac{h_c R}{k}\right)\right)\cdot\frac{\alpha\theta}{R^2}\right)+\frac{2\alpha\theta}{R^2}\right\} / \left(2\alpha\,(1+\left(\frac{h_c R}{k}\right))\right) \tag{18}$$

and,

$$Q_r = 4\pi R^2 h_r \varphi_B \cdot \theta \cdot \left(1-\alpha\theta h_r/(Rk)\right) \tag{19}$$

with the radiation result based on a time integration of the solution presented in [16]. Trend lines representative of both results, are presented in Fig. 7, pertinent to a 0.05 m radius bubble undergoing cooling with T_B = 4500 K and T_∞ = 811K and concentric sphere configuration used in radiation modelling. Assuming that homogeneous condensation or radiative cooling through a fog layer was not present, one can infer from these trends, that sufficient heat transfer took place during the cooling phase to dissipate, by a significant margin, the energy supplied during capacitor discharge, provided the mode of heat transfer

was radiation to the bubble surface. This assessment is based on a comparison of the bubble rise time, computed using the Taylor formula,

$$\theta = H/\sqrt{gR} \qquad (20)$$

against the elapsed time required for energy transfer out of the bubble, with this second time being determined by entering the trend lines of Fig. 7 with an ordinate value that is equivalent to the CDV energy input for that test, as listed in Table I. To illustrate how this assessment was made, consider test 104. With a CDV energy input of 37.4 kJ, one could infer, assuming no other energy transfers are taking place, that radiative cooling was sufficient to accommodate the reported CDV energy input. The inference is based on a comparison of two time predictions: a time prediction from Fig. 7 of 0.4 s for radiative heat transfer to accrue to a level of 37 kJ, against a 1.07 s evaluation of rise time using (20). It could be argued, based on these time values, that the energy level of the sample material, met a time requirement for returning to a starting energy level that was well within the predicted rise time for a bubble buoying up through the coolant so that the bubble may have been energetically spent shortly after capacitor discharge so as to be incapable of transporting significant amounts of aerosol to the covergas. It could then be inferred that the vapor contents of the bubble at the time of release to the covergas were mainly non-condensables. From this reasoning, one could further argue that the UO_2 vapor had time to condense while the bubble was buoying up; time was not sufficient to permit significant aerosol transport to the covergas. Furthermore, predicted boundary work, depicted in Fig. 8 for each sodium experiment, suggests that this energy transfer, although contributing to the energy balance and reported with scatter about the kilojoule level was not sufficiently present to justify reassessing the overall claim that heat transfer from the bubble was the dominant mode of energy exchange. It should also be noted that, if surface condensation could be made to occur early, it might not be possible to sustain the claim that bubble transport to the covergas was unlikely, since the curve in Fig. 7 pertaining to condensation is seen to have a much lower slope. As a result, a significantly greater time would be needed to achieve dissipation of the energy input, for this case where radiation was absent. Extrapolations from the condensation result presented in Fig. 7 suggest time requirements of 3.5 s or greater would be needed to transfer 37.4 kJ of energy out, exceeding, by a factor of 3, the time available for bubble transit to the cover gas. Therefore, both the role of condensation in sustaining bubble transport, and

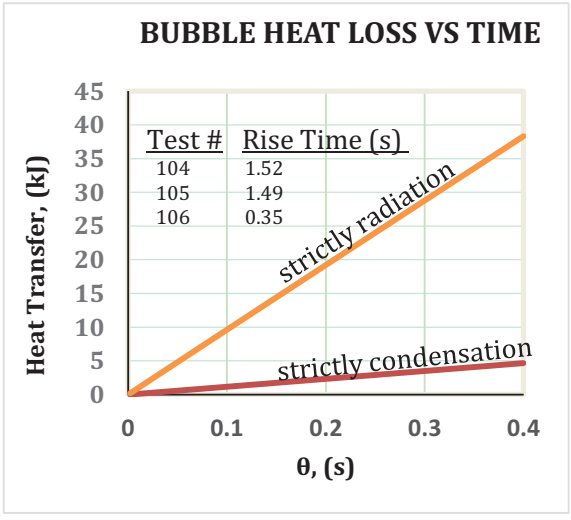

Figure 7. Comparison of Heat Transfer Modes
(h_c , h_r = 100, 830 ; ε_{UO2} , ε_{Na} = 0.28 , 0.20)

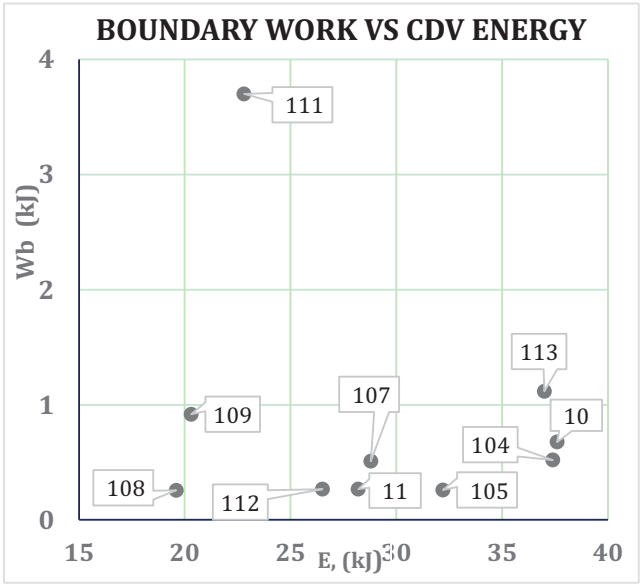

Figure 8. Work Transfer Trends (Na Tests)

means for assessing the cut-in time for condensation heat transfer require further study. In addition, the possibility that more complicated heat transfer models, such as those accounting for homogeneous nucleation, with subsequent radiation heat transfer through a fog layer, might also bring about a satisfactory overall energy balance, cannot at this time be ruled out.

6. CONCLUSIONS

Data obtained from out-of-reactor source term experiments conducted in the Fuel Aerosol Simulant Test facility at Oak Ridge National Laboratory have been assessed from the perspective of coolant-bubble-covergas energetics for purposes of explaining the low level of aerosol release observed in many of the experiments. Considering three types of energy transfer thought to be present, a rank ordering from most to least energetic suggested that radiative heat transfer, at least during the early stages of event progression, may have been 7 to 8 times more energetic than condensation heat transfer, which in turn may have been 4 to 5 times more energetic than work transfer. This could suggest that the effectiveness of radiative cooling led to wholesale condensation of the volatile components, perhaps in a bulk or homogeneous nucleation, occurring while the bubble was submerged within the pool. The trace amounts of aerosol material released from the pool under these conditions would be due to noncondensable gas buoying up through the coolant. Additionally, results of a condensation heat transfer assessment, using a time dependent heat transfer model formulated for a spherical volume of coolant adjoining the bubble, suggested that if condensation heat transfer cut-in early, the cooling of the bubble could be sufficiently delayed so that a buoyant bubble containing aerosols would be more likely to reach the covergas. Since observed release levels were extremely low, it does not seem probable that condensation heat transfer served as a rate limiting mode. Nonetheless, should a licensing case need to be made for an oxide-fueled liquid metal-cooled reactor, a more detailed assessment of these experiments could be warranted with an effort directed at developing a means of assessing the cut-in time for surface condensation. To make the modelling more complete with respect to radiation, identified as the most probable, dominant mode in this study, an extension of the physical configuration to include the presence of a fog or particulate layer may be needed. The presence of a fog layer may reduce radiation heat transfer thereby increasing bubble lifetimes and subsequent transport of aerosol to the covergas, significantly altering the claim that radiation strongly impedes bubble transport towards the covergas.

The results reported here contribute to an evaluation of previously developed experimental efforts aimed at establishing a more mechanistic source term assessment. Because statements regarding the behaviour of these bubble types have largely remained speculative and with gap analyses [3] duly noting the need for more specificity regarding the underlying rationale associated with source term estimation, the models presented here could serve as a useful baseline check to be utilized in more sophisticated code development that may need to be performed in addressing the safety case associated with advanced liquid metal cooled reactors.

NOMENCLATURE

upper case
H, pool level relative to the vaporizer, (m)
P, pressure, (Pa)
R, bubble radius, (m)
T, temperature, (K)
T_i, initial temperature level of coolant, (K)
V, volume, (m^3)
W, work transfer, (J)

lower case
c_p, constant pressure specific heat , (J/kg-K)
g, gravitational acceleration, (m/s^2)
h, depth of vaporizer, initial depth of bubble, (m)
h_c, condensation heat transfer coefficient, (W/m^2-K)
h_r, radiation heat transfer coefficient, (W/m^2-K)
k, thermal conductivity, (W/m-K)

q", heat flux, (W/m^2)
r, radial offset from system center, (m)
t, transformed temperature group, (K-m)
z, bubble displacement, (m)

Greek
α, thermal diffusivity, (m^2/s)
β, similarity variable (dimensionless)
γ, specific heat ratio, (dimensionless)
δ, e-folding length, (m) [Distance over which the exponential function diminishes by a multiplicative factor of 0.3678… i.e., e^{-1}.]
Δ , the change in a quantity ≡ final – initial,
ε, coolant emissivity (dimensionless)
∇^2 , Laplacian operator
η, aerosol release indicator (dimensionless)
ρ, density, (kg/m^3)
ρc_p , volumetric thermal inertia, (J/m^3-K)
θ, time, (s)
φ, excess coolant temperature, (K)

subscripts
cg, covergas quantity
c, a condensation heat transfer quantity
con, a heat conduction quantity
0, baseline quantity
max, maximum value
r, a radiation heat transfer quantity
R, quantity evaluated at r = R
B, bubble related quantity
∞, far-field quantity

ACKNOWLEDGEMENT

JCP expresses appreciation to Tony Wright, Oak Ridge National Laboratory (retired), for helpful discussions regarding aspects of the preliminary water experiments reported in this paper.

REFERENCES

1. A. Brunett, R. Denning, M. Umbrel, W. Wutzler, "Severe Accident Source Terms for a Sodium-cooled Fast Reactor", *Annals of Nuclear Energy*, **64 ,** pp. 220-229 (2014).
2. F. J. Arias, G. T. Parks, "An Estimate of the Order of Magnitude of the Explosion during a Core Meltdown-Compaction Accident for Heavy Liquid Metal Fast Reactors: A Disquieting Result Updating the Bethe-Tait Model", *Progress in Nuclear Energy*, **79**, pp. 182-189, (2015).
3. D. A. Powers, B. Clement, R. Denning, S. Ohno, R. Zeyen, *Advanced Sodium Fast Reactor Source Terms: Research Needs*, SAND2010-5506, Sandia National Laboratory, (2010).
4. A. Minato, N. Ueda, D. Wade, E. Greenspan, N. Brown, *Small Liquid Metal Cooled Reactor Safety Study*, UCRL-TR-217093, Lawrence Livermore National Laboratory, (2005).
5. G. F. Flanagan, G. T. Mays, I. K. Madni, "*NRC Program on Knowledge Management for Liquid-Metal Cooled-Reactors",*NUREG/KM-0007(ORNL/TM-2013-79) , US Nuclear Regulatory Commission, Washington, DC (2014).
6. G. Berthoud, A. W. Longest, A. L. Wright, W. P. Schutz, "Experiments on Liquid-Metal Fast Breeder Reactor Aerosol Source Terms After Severe Accidents", *Nuclear Technology*, **81,** pp. 257-277 (1988).
7. J. C. Petrykowski, A. W. Longest, J. M. Rochelle, A. L. Wright, *Aerosol Release Experiments in the*

Fuel Aerosol Simulant Test Facility: Under Sodium Experiments, ORNL/TM-9479, Oak Ridge National Laboratory, Oak Ridge, TN (1985).
8. A. L. Wright, A. M. Smith, J. M. Rochelle, T. S. Kress, *Fuel Aerosol Simulant Test Data Record Report: Underwater Tests,* ORNL/TM-8085, Oak Ridge National Laboratory, Oak Ridge, TN (1982).
9. J. R. Blake, D. C. Gibson, "Growth and Collapse of a Vapor Cavity Near a Free Surface", *J. Fluid Mech.* **111**, pp. 123-40, (1981).
10. M. N. Ozisik, T. S., Kress, "Effects of Internal Circulation Velocity and Noncondensable Gas on Vapor Condensation from a Rising Bubble", *Nuclear Science and Engineering*: **66**, 397-405 (1978).
11. M. L. Tobias, "Analysis of the Heat and Mass Transfer Processes of a UO_2 Bubble in Sodium*"*. *Proceedings of the International Meeting on FAST Reactor Safety Technology*, Seattle, (1979).
12. M. L. Tobias, "*Analysis of the Heat and Mass Transfer Processes of a UO_2 Bubble in Sodium for the Fuel Aerosol Simulant Test (FAST)",* NUREG/CR-0678; ORNL/NUREG/TM-307, Oak Ridge National Laboratory, Oak Ridge, TN (1979).
13. A. B. Reynolds, D. R. Bradley, J. Y. Ku, R. L. Webb, " The UVABUBL Program and its Application to the FAST Underwater Tests", *Nucl. Engrng. Des*. , **105,** pp**.** 199-222 (1988).
14. R. Clift, J. R. Grace, and M. E. Weber. "*Bubbles, Drops and Particles*" Academic Press New York, New York, (1978).
15. J. C. Petrykowski, A. L. Wright, Y. Shi, " Nucleate Boiling Theory for Gaging Fuel-Coolant Interaction Potential Associated with LMR Source Term Experiments", *(NURETH15),* Pisa, Italy, May 12-17, 2013, Paper #675.
16. J. C. Petrykowski, "Analysis of Fuel-coolant Interaction Potential in Sodium Cooled Fast Reactor Safety Experiments", *Proceedings of the 20th International Conference on Nuclear Engineering (ICONE20), Article ID 54925,* Anaheim, CA, (2012).
17. M. L. Corradini, W. M. Rohsenow, N. E. Todreas, "The Effects of Sodium Entrainment and Heat Transfer with Two-phase UO2 During a Hypothetical Core Disruptive Accident", *Nuclear Science and Engineering*, **73**, pp. 242-258 (1980).
18. M. R. Spiegel, S. Lipschutz, J. Liu, *Mathematical Handbook of Formulas and Tables,* 3rd edn, p. 203, McGraw-Hill, New York, NY (2009).
19. J. K. Fink, M. G. Chasanov, and L. Leibowitz, "*Properties for Reactor Safety Analysis*", ANL-CEN-RSD-82-2, Argonne National Laboratory, Argonne, IL (1982).
20. F. P. Incropera, D. W. DeWitt, T. L. Bergman, A. S. Lavine, *Fundamentals of Heat and Mass Transfer,* 6th edn, John Wiley, New York (2007).
21. D. H. Cho, D. W. Condiff, S. H. Chan, "Role of Fuel Bubble Phenomenology in Assessment of LMFBR Source Term", Proceedings of ANS/ENS Fast Reactor Safety Meeting, Knoxville, Tennessee, April 21-25, 1985 pp. 827-833, (1985).

APPENDIX A

Determination of bubble size from covergas pressure measurements begins by noting that for an incompressible coolant the covergas and bubble undergo compensating changes in volume so that,

$$\Delta V_B = -\Delta V_{cg} \quad . \tag{A-1}$$

Based on this change in bubble volume the current bubble volume becomes,

$$V_B = V_{B_0} + \Delta V_B. \tag{A-2}$$

The covergas volume change can be related to covergas pressure readings through the 3rd isentropic property relation,

$$(PV^{\gamma})_{cg_0} = (PV^{\gamma})_{cg} \tag{A-3}$$

which can be solved for the current covergas volume viz.,

$$V_{cg} = V_{cg_0} \cdot \left(\frac{P_{cg_0}}{P_{cg}}\right)^{1/\gamma}. \tag{A-4}$$

Then, in three steps, the bubble volume results,

first, $$\Delta V_{cg} = V_{cg} - V_{cg_0}, \tag{A-5}$$

then, $$\Delta V_{cg} = V_{cg_0} \cdot \left(\left(\frac{P_{cg_0}}{P_{cg}}\right)^{1/\gamma} - 1\right) \tag{A-6}$$

which leads to, $$V_B = V_{B_0} - V_{cg_0} \cdot \left(\left(\frac{P_{cg_0}}{P_{cg}}\right)^{1/\gamma} - 1\right). \tag{A-7}$$

Finally, using the volume formula for a sphere, the bubble radius becomes,

$$R = \sqrt[3]{\frac{3}{4\pi}\left(V_{B_0} + V_{cg_0}\left(1 - (P_0 / P)_{cg}^{1/\gamma}\right)\right)} \tag{A-8}$$

which matches equation (1) presented in Sect 3.1 of the text.